Proceedings of the 2006 American Control Conference
Minneapolis, Minnesota, USA, June 14-16, 2006

CFD-Based Adaptive Flow Control Using ARMARKOV Disturbance Rejection

Matthew A. Rizzo[†], Mario A. Santillo[†], Ashwani K. Padthe[†], Jesse B. Hoagg[†], Suhail Akhtar[‡], Kenneth Powell[†] and Dennis S. Bernstein[†]

[†]Department of Aerospace Engineering
University of Michigan, Ann Arbor, MI 48109
{marizzo, santillo, akpadthe, jhoagg, powell, dsbaero}@umich.edu

[‡]National University of Science & Technology
Pakistan
suhail-cae@nust.edu.pk

I. Introduction

In this paper we demonstrate adaptive flow control for an incompressible viscous fluid through a two-dimensional channel without the use of an analytical model. An adaptive disturbance rejection algorithm is implemented within a CFD simulation to reduce the effects of an unknown velocity disturbance on the performance variable z, which is the transverse velocity component of the flow at a downstream location. The algorithm requires minimal knowledge of the system, specifically, the numerator coefficients of the transfer function from the control input to the performance variable. System identification, based on CFD simulations prior to the disturbance rejection simulations, is used to identify the required parameters.

Adaptive flow control is achieved using the ARMARKOV disturbance rejection algorithm [1], [2] implemented within the CFD software Fluent, a commercial computational fluid dynamics software package available from Fluent, Inc [3]. The ARMARKOV algorithm has been applied to various testbeds in [4]–[12]. We consider a two-dimensional channel geometry with two velocity sensors y and z and one control jet u. The goal is to reduce the effects of an unknown disturbance upstream using the control jet positioned between the two sensors. This arrangement is motivated by [13], which suggests that spillover can be avoided if the control jet and the disturbance source are noncolocated and if the performance sensor and measurement sensor are also noncolocated.

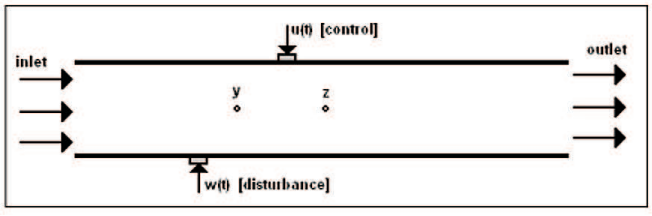

Fig. 1. 2D channel geometry for adaptive flow control. The objective of the control problem is to suppress the transverse flow velocity at z.

Supported by the National Aeronautics and Space Administration under a Graduate Researchers Program Fellowship

An overview of flow control is given by [14]. Many standard control techniques have been applied to active flow control. For example, PI and LQG controllers have been considered in [15]–[17] based on a reduced-order model of the linearized Navier-Stokes equation, obtained by a Galerkin procedure. LQG/LTR control of the streamfunction formulation of the Navier-Stokes equation is used in [18], [19] to achieve drag reduction below the laminar level. An LQG controller based on a reduced-order model obtained from a finite element code is used in [20]. In addition, a nonlinear control law is developed in [21], where a Galerkin method is used to derive a reduced-order model of the two-dimensional Navier-Stokes equation. Alternative methods presented in [22]–[24] include PDE-based control, robust control, and predictive control with direct numerical simulation.

Flow control using ARMARKOV disturbance rejection differs from model-based control methods since a detailed model of the flow is not required. Instead, a CFD simulation is used to generate input/output data of the flow while band-limited white noise is applied at the control jet. The numerator coefficients of an ARMARKOV model are then identified off-line using the Matlab System Identification Toolbox. The combination of CFD simulation and the ARMARKOV disturbance rejection algorithm thus constitutes a technique for controlling a fluid without analytical modeling. Adaptive flow control is achieved by means of a compensator whose parameter matrix is updated on-line by a gradient algorithm so that disturbance rejection is achieved.

To apply this technique to a physical system one would first use a CFD simulation coupled with system identification to obtain the numerator coefficients of an ARMARKOV model of the system. Adaptive disturbance rejection using the ARMARKOV algorithm could then be implemented in real time on the physical system. Alternatively, measurements obtained from the physical system can be used for identification assuming that the disturbance level is manageable compared to the control input.

II. Problem Statement and Description

Consider the 2D channel geometry shown in Figure 1. Let $w(t) \in \mathbb{R}$ be the transverse disturbance to the nominal

laminar flow, $u(t) \in \mathbb{R}$ the control signal applied to the flow, $y(t) \in \mathbb{R}$ the measurement variable, and $z(t) \in \mathbb{R}$ the performance variable. Here $y(t)$ and $z(t)$ are the transverse velocity components of the flow at the sensor locations. Both $w(t)$ and $u(t)$ represent mass flow into (or out of) the system.

The goal of this paper is to demonstrate the use of ARMARKOV disturbance rejection adaptive flow control based directly on a CFD simulation of 2D channel Poiseuille (viscous) flow. Two suction/blowing jets are placed in the walls of the channel, one that applies the disturbance (located 0.75 m from the inlet on the lower wall) and the second to control the disturbed flow (located 1.25 m from the inlet on the upper wall). Two transverse velocity sensors are located in the center of the channel 0.25 m downstream from each jet. The wall separation distance is 0.25 m. For the purpose of simulation, we take the channel centerline velocity to be 2 m/s and the fluid to be incompressible. Taking the fluid as air at standard temperature and pressure and wall separation as the characteristic length, the Reynolds number is 3.3×10^4.

A segregated, 2D, unsteady, implicit solver is used for the CFD simulation, along with User Defined Functions (UDFs) and function hooks to integrate the custom C-programming code into the simulation. ASCII text files are used to transfer necessary data to and from the simulation environment.

III. Adaptive Disturbance Rejection Algorithm Description

Consider the n^{th}-order discrete-time finite-dimensional linear time-invariant TITO system

$$x(k+1) = Ax(k) + Bu(k) + D_1 w(k) \quad (1)$$
$$z(k) = E_1 x(k) + E_2 u(k) + E_0 w(k) \quad (2)$$
$$y(k) = Cx(k) + Du(k) + D_2 w(k) \quad (3)$$

or in a transfer function representation

$$z = G_{zw} w + G_{zu} u \quad (4)$$
$$y = G_{yw} w + G_{yu} u. \quad (5)$$

The controller G_c that produces the control signal $u(k)$ using feedback $y(k)$ can be written as

$$u = G_c y + G_{zu} u. \quad (6)$$

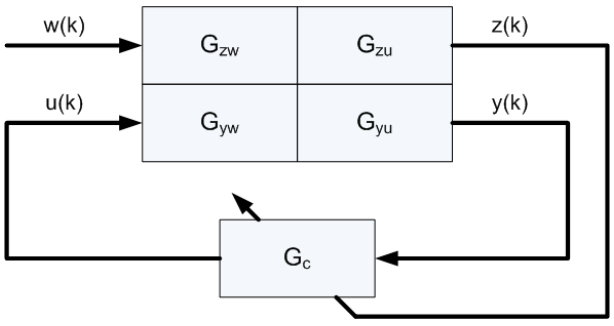

Fig. 2. Standard problem with controller adaptation

The ARMARKOV model of (1) - (3) is given by

$$\begin{aligned} z(k) = &\sum_{j=1}^{n} -\alpha_j z(k-\mu-j+1) \\ &+ \sum_{j=1}^{\mu} H_{zw,j-2} w(k-j+1) \\ &+ \sum_{j=1}^{n} B_{zw,j} w(k-\mu-j+1) \\ &+ \sum_{j=1}^{\mu} H_{zu,j-2} u(k-j+1) \\ &+ \sum_{j=1}^{n} B_{zu,j} u(k-\mu-j+1) \end{aligned} \quad (7)$$

$$\begin{aligned} y(k) = &\sum_{j=1}^{n} -\alpha_j y(k-\mu-j+1) \\ &+ \sum_{j=1}^{\mu} H_{yw,j-2} w(k-j+1) \\ &+ \sum_{j=1}^{n} B_{yw,j} w(k-\mu-j+1) \\ &+ \sum_{j=1}^{\mu} H_{yu,j-2} u(k-j+1) \\ &+ \sum_{j=1}^{n} B_{yu,j} u(k-\mu-j+1) \end{aligned} \quad (8)$$

with the Markov parameters of the system being

$$H_{yu,-1} \triangleq D, \quad H_{yu,j} \triangleq CA^j B, \quad j \geq 0 \quad (9)$$
$$H_{yw,-1} \triangleq D_2, \quad H_{yw,j} \triangleq CA^j D_1, \quad j \geq 0 \quad (10)$$
$$H_{zu,-1} \triangleq E_2, \quad H_{zu,j} \triangleq E_1 A^j B, \quad j \geq 0 \quad (11)$$
$$H_{zw,-1} \triangleq 0, \quad H_{zw,j} \triangleq E_1 A^j D_1, \quad j \geq 0 \quad (12)$$

where α_j, $B_{zw,j}$, $H_{zw,j}$, $B_{zu,j}$, $H_{zu,j}$, $B_{yw,j}$, $H_{yw,j}$, $B_{yu,j}$, and $H_{yu,j} \in \mathbb{R}$, $j = 1, \ldots, n$.

Next, define the *extended performance vector* $Z(k)$, the *extended measurement vector* $Y(k)$ and the *extended control vector* $U(k)$ by

$$Z(k) \triangleq \begin{bmatrix} z(k) \\ \vdots \\ z(k-p+1) \end{bmatrix}, Y(k) \triangleq \begin{bmatrix} y(k) \\ \vdots \\ y(k-p+1) \end{bmatrix}$$
$$U(k) \triangleq \begin{bmatrix} u(k) \\ \vdots \\ u(k-p_c+1) \end{bmatrix} \quad (13)$$

where $p_c \triangleq \mu + n + p - 1$, and the ARMARKOV

regressor vectors $\Phi_{zw}(k)$ and $\Phi_{yw}(k)$ by

$$\Phi_{zw}(k) \triangleq \begin{bmatrix} z(k-\mu) \\ \vdots \\ z(k-\mu-p-n+2) \\ w(k) \\ \vdots \\ w(k-\mu-p-n+2) \end{bmatrix}$$

$$\Phi_{yw}(k) \triangleq \begin{bmatrix} y(k-\mu) \\ \vdots \\ y(k-\mu-p-n+2) \\ w(k) \\ \vdots \\ w(k-\mu-p-n+2) \end{bmatrix}. \quad (14)$$

Furthermore, define the block-Toeplitz ARMARKOV *weight matrices* $W_{zw}, W_{yw} \in \mathbb{R}^{p\times[2(n+p-1)+\mu]}$ and block-Toeplitz ARMARKOV *control matrices* $B_{zw}, B_{yw} \in \mathbb{R}^{p\times p_c}$, as described in [1]. Then (7) and (8) can be written in the form

$$Z(k) = W_{zw}\Phi_{zw}(k) + B_{zu}U(k) \quad (15)$$

$$Y(k) = W_{yw}\Phi_{yw}(k) + B_{yu}U(k) \quad (16)$$

which is the ARMARKOV/Toeplitz model of (1) - (3).

The adaptive disturbance rejection algorithm for the TITO system represented in (15) and (16) uses a strictly proper controller in ARMARKOV form of order n_c and μ_c Markov parameters, so that, analogous to (7) and (8), the control $u(k)$ is given by

$$\begin{aligned} u(k) = &\sum_{j=1}^{n_c} -\alpha_{c,j}(k)u(k-\mu_c-j+1) \\ &+ \sum_{j=1}^{\mu_c-1} H_{c,j-1}(k)y(k-j+1) \\ &+ \sum_{j=1}^{n_c} B_{c,j}(k)y(k-\mu_c-j+1) \end{aligned} \quad (17)$$

where $H_{c,j} \in \mathbb{R}$, $j = 1, 2, \ldots$, are the Markov parameters of the controller. Next, define the *controller parameter block vector* $\theta(k) \in \mathbb{R}^{1\times[2n_c+\mu_c-1]}$ by

$$\begin{aligned} \theta(k) \triangleq [&-\alpha_{c,1}(k), \ldots, -\alpha_{c,n_c}(k), H_{c,0}(k), \\ &\ldots, H_{c,\mu_c-2}(k), B_{c,1}(k), \ldots, B_{c,n_c}(k)]. \end{aligned} \quad (18)$$

Now from (17) it follows that $u(k)$ is given by

$$u(k) = \theta(k)R_1\Phi_{uy}(k) \quad (19)$$

where $R_1 \in \mathbb{R}^{[2n_c+\mu_c-1]\times[2(n_c+p_c-1)+\mu_c-1]}$ is a picking matrix with the form described in [1].

Finally, the update law for the controller parameters is given by

$$\theta(k+1) = \theta(k) - \eta(k)\frac{\partial J(k)}{\partial\theta(k)} \quad (20)$$

where $\eta(k)$ is the *adaptive step size*. (20) is derived in [1] along with all additional steps.

IV. System Identification for a Linearized Flow Model

To obtain the required controller parameters for the ARMARKOV model, a CFD simulation is used with band-limited white noise injected into a near nominal (undisturbed) laminar flow from the control jet. Both the input and performance velocity measurement are recorded at a sampling rate of 100 Hz.

The linear model estimation function "pem" in the Matlab System Identification Toolbox is used to obtain a linear model of the perturbed dynamics about the nominal flow. The "pem" function computes the prediction error estimate of a general linear model using input/output data, and then returns an estimated model. To independently verify the model obtained from the "pem" function, the Matlab function "tfestimate" is used. The "tfestimate" function estimates the transfer function of the system given input/output data using Welch's averaged periodogram method. Here, the identified ARMARKOV model is a sixth order system. Figure 3 shows the Bode magnitude plot from both methods.

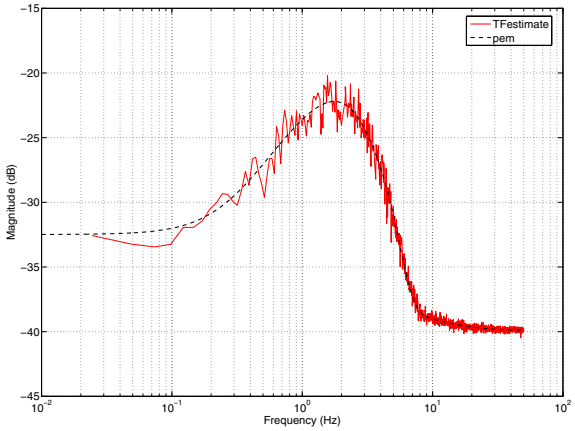

Fig. 3. Identified transfer functions from control input $u(t)$ to performance variable $z(t)$ using CFD generated data. The Matlab 'tfestimate' function and the System Identification Toolbox function 'pem' plots are both shown.

From the frequency response plot in Figure 3 it is seen that the channel dampens out all but a small frequency band from approximately 1 Hz to 4 Hz. Likewise, the channel attenuates input signals from the control jet to the performance measurement position. These characteristics, which are related to the geometry of the channel, are needed by the adaptive algorithm to control the flow.

V. Results

Three types of CFD simulations are used to test the adaptive disturbance rejection algorithm. In all three cases a transverse velocity disturbance is applied to the flow upstream from both sensors and from the control jet. Although the disturbance is created within the simulation, the controller has no knowledge of the disturbance.

The CFD mesh is a rectangular grid with cell size 0.01 m $\times$ 0.01 m, resulting in 300 streamwise cells and 25 wall

normal cells. The simulation step size is 0.01 s. Multiple simulations were run with different space and time discretizations to determine appropriate values for maintaining the underlying fluid dynamics.

The amplitude of the injected disturbance signal w is chosen to be 75% of the channel centerline velocity. The control input u is updated directly from the adaptive algorithm. In all simulations, the amplitude of the control input stays below about 50% of the disturbance signal amplitude.

We first use a single tone signal to disturb the nominal flow in the channel. A sine wave with constant frequency and constant amplitude is applied to a velocity inlet within the CFD simulation. Using the Fluent User Defined Functions (UDFs) a C-program function was written and connected to the simulation. At every time step within the simulation the boundary condition at the disturbance control jet is set according to the output of the disturbance UDF. The second method uses the same configuration within Fluent except the applied disturbance signal has two sinusoids driving the jet. Finally, the third method uses a band-limited noise signal to disturb the flow. The band-limited noise signal is produced prior to the CFD simulation using a Matlab Simulink model and then saved to an ASCII text file. The text file is read during the simulation and applied at the disturbance jet.

A nominal horizontal flow in the center of the channel of 2 m/s is used for all simulations while the frequencies and amplitudes of the disturbance are varied to test the controller. In addition to varying the disturbance properties, the order of the controller is also varied.

Figure 4 shows the time history of the transverse velocity $z(t)$ of both the open-loop and closed-loop response to a disturbance signal at 2.5 Hz. The adaptive disturbance rejection controller decreases the transverse velocity within a few seconds. Only low amplitude higher frequency components remain once the controller converges. Figure 5 shows the power spectral density of both the open-loop response and the closed-loop response. A reduction of more than 80 dB is achieved at the disturbance frequency of 2.5 Hz. Due to the nonlinearity of the flow dynamics multiple harmonics remain, however, the power at these frequencies is less than at the 2.5 Hz fundamental frequency.

The results shown in Figures 4 and 5 are obtained with a controller order of 10. The controller order was varied between 10 and 20. As the controller order was increased, further disturbance rejection was not generally obtained.

In addition to varying the controller order, the effect of varying the frequency of the disturbance was also investigated. Adaptive disturbance rejection was achieved for a frequency band between 2 Hz and approximately 6 Hz with a controller order of 10. Increasing the controller order increased the higher frequency limit slightly. Above 6 Hz the channel tends to dampen the transverse velocity component from the disturbance w to the performance z, so no control is necessary for higher frequency disturbances.

Figure 6 shows relative velocity vector plots of the flow within the channel. The reference velocity vector was chosen to be the nominal flow vector at the center of the channel (2 m/s in the horizontal direction). Open-loop and closed-loop flows are shown.

For the open-loop case it can be seen that the velocity at the performance position, along with positions downstream, have large transverse velocity components. However, in the closed-loop case the transverse velocity components of the flow at and downstream from the performance position are small due to actuation by the control jet. Small transverse velocity components, in the closed-loop case, of the flow downstream from the performance position are due to the channel's dampening characteristic. However, for this to happen the controller must first be able to reduce the transverse velocity at the performance position.

Dual frequency disturbance rejection was simulated in a similar manner as in the single frequency case, with the only change being in the UDF's used to drive the disturbance jet. Figure 7 shows the time history of both the open-loop and closed-loop response to a disturbance containing 2 Hz and 6 Hz components. The controller can be seen to reduce the amplitude of the transverse velocity in the performance variable z in about 10 seconds. Figure 8 shows the power spectral density plot of the open-loop and closed-loop response to the dual tone disturbance. A decrease of up to 80 dB is seen in both frequencies, as well as with the higher harmonics.

As with the single tone case, both the frequencies of the disturbance and the controller order were varied. Although the majority of frequency pairs between 2 Hz and 6 Hz were rejected by the controller, there exist cases where disturbance rejection was not obtained. The nonlinear effect of the channel flow dynamics in some cases produced strong super and sub harmonics that were not removed by the controller. In these cases the magnitude of the closed-loop performance is less than the open-loop response but not to the degree shown in Figure 7.

Varying controller order for the dual-tone case was found

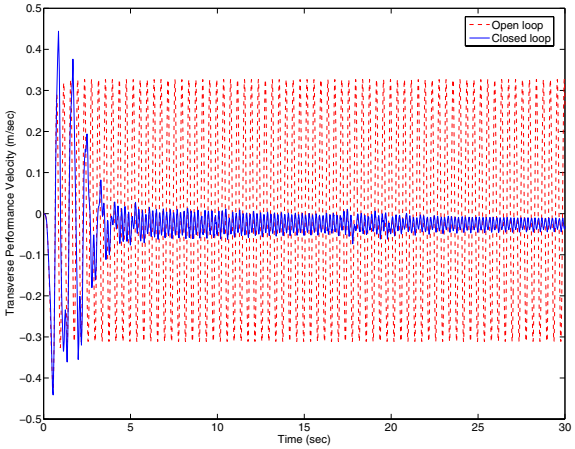

Fig. 4. Open-loop and closed-loop transverse performance velocity response for a single tone 2.5 Hz disturbance rejection with controller order n_c = 10.

to have both a positive and negative effect. In the particular case of a 2 Hz and 6 Hz dual-tone disturbance, as the controller order is increased from $n_c = 12$, the rejection of the fundamental frequencies stays nearly the same, however, spillover occurs at both super and sub harmonics. This spillover led to an overall larger magnitude steady-state response of the transverse performance variable z, and in some cases caused the simulation to fail. In most simulations a controller order was found that had good reduction of the fundamental frequencies with a reasonable attenuation of both super and sub harmonics.

The third case tested used band-limited white noise as the disturbance signal. The disturbance signal was limited to a frequency band of approximately 2 Hz to 6 Hz. Based on the single tone and dual tone experiments described above, the system was expected to reduce the effects of disturbances within the narrow 1 Hz to 4 Hz window.

Figures 9 and 10 show the power spectral density plots obtained from the CFD simulation. Both plots show decreased power between approximately 1.5 Hz and 3 Hz. Figure 10 is the response using a larger controller order, n_c = 19, than in Figure 9, where n_c = 12. Experiments conducted using controller orders above 20 were not successful. As in the single and dual tone cases, a controller order between these extremes seems to produce the best results.

In addition to trying different controller orders, the amplitude of the band-limited white noise disturbance was increased. It was found that the higher amplitude excited the nonlinear dynamics of the flow, which the controller was not able to suppress by a substantial amount. Channel flow can be excessively sensitive to external perturbations for moderate Reynolds number, including transient energy growth, subcritical bifurcations, transition to chaos, and turbulence [25]. Future analysis will focus more directly on controller sensitivity to flow properties and controller order.

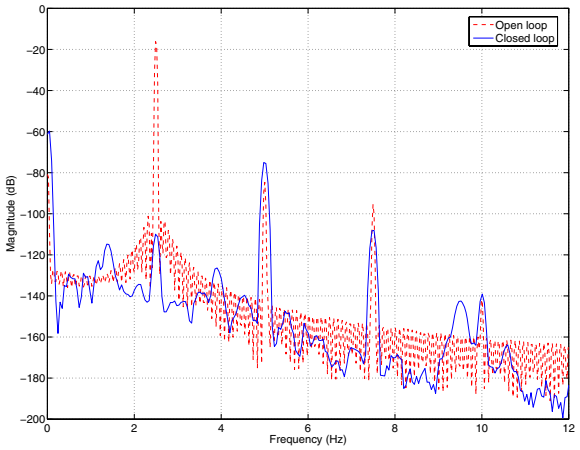

Fig. 5. Open-loop and closed-loop power spectrum for a single tone 2.5 Hz disturbance with controller order n_c = 10. A decrease of more than 80 dB at the disturbance frequency is shown with all other frequency content at least 60 dB below the strongest open loop signal.

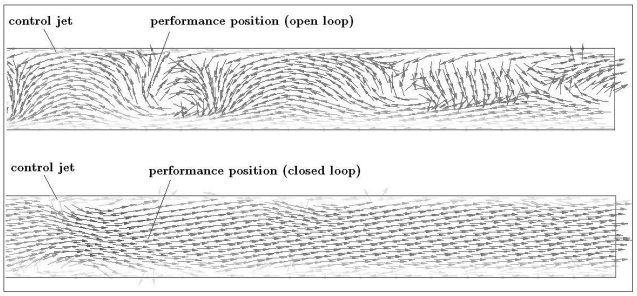

Fig. 6. Relative velocity vector plots of the open-loop and closed-loop flows. The velocity vectors are relative to the 2 m/s horizontal nominal flow. These plots show the right-hand half of the channel to compare the open and closed loop flows. The flow simulations are obtained from the CFD simulation software Fluent.

VI. Conclusion

Adaptive flow control using the ARMARKOV disturbance rejection algorithm was demonstrated by means of a 2D channel Poiseuille flow CFD simulation. System identification was used to estimate the numerator coefficients of the transfer function from the control input to the performance variable. No analytical model was derived or is needed for this adaptive disturbance algorithm. Disturbance rejection was demonstrated for single-tone, dual-tone, and band-limited white noise disturbances. Disturbance rejection of up to 80 dB, between 2 Hz and 6 Hz, for both the single-tone and dual-tone cases was achieved, along with up to 40 dB rejection, between 1.5 Hz and 3 Hz, in the band-limited white noise case.

References

[1] R. Venugopal and D. S. Bernstein, "Adaptive disturbance rejection using ARMARKOV/Toeplitz models," *IEEE Trans. Contr. Syst. Technol.*, vol. 8, no. 2, pp. 257–269, 2000.

[2] S. Akhtar and D. Bernstein, "Discrete-time adaptive stabilization and disturbance rejection for minimum phase plants," in *Proc. Conf. Dec. Contr.*, Seville, Spain, 2005, pp. 2236–2241.

[3] "CFD Flow Modeling Software," Fluent Inc., February 2006, http://www.fluent.com/.

[4] J. C. Akers and D. S. Bernstein, "ARMARKOV least-squares identification," in *Proc. Amer. Contr. Conf.*, Albuquerque, NM, June 1997, pp. 186–190.

[5] ——, "Time-domain identification using ARMARKOV/Toeplitz models," in *Proc. Amer. Contr. Conf.*, Albuquerque, NM, June 1997, pp. 191–195.

[6] S. Akhtar and D. S. Bernstein, "Optimal adaptive feedback disturbance rejection," in *Proc. ACTIVE 04*, Williamsburg, VA, September 2004.

[7] J. Chandrasekar, L. Liu, D. Patt, P. P. Friedmann, and D. S. Bernstein, "Active noise cancellation for systems with uncertain dynamics using adaptive harmonic steady state control," in *Proc. ACTIVE 04*, Williamsburg, VA, September 2004.

[8] J. B. Hoagg and D. S. Bernstein, "Discrete-time adaptive feedback disturbance rejection using a retrospective performance measure," in *Proc. ACTIVE 04*, Williamsburg, VA, September 2004.

[9] J. B. Hoagg, S. L. Lacy, R. Venugopal, and D. S. Bernstein, "Adaptive control of a flexible membrane using acoustic excitation and optical sensing," in *AIAA Guid. Nav. Contr. Conf.*, Austin, TX, August 2003, AIAA-2003-5430.

[10] S. L. Lacy, R. Venugopal, and D. S. Bernstein, "ARMARKOV adaptive control of self-excited oscillations of a ducted flame," in *Proc. Conf. Dec. Contr.*, Tampa, FL, December 1998, pp. 4527–4528.

[11] H. Sane and D. S. Bernstein, "Active noise control using an acoustic servovalve," in *Proc. Amer. Contr. Conf.*, Philadelphia, PA, June 1998, pp. 2621–2625.

[12] H. Sane, R. Venugopal, and D. S. Bernstein, "Disturbance rejection using self-tuning ARMARKOV adaptive control with simultaneous identification," *IEEE Trans. Contr. Sys. Tech.*, vol. 9, pp. 101–106, 2001.
[13] J. Hong and D. S. Bernstein, "Bode integral constraints, colocation, and spillover in active noise and vibration control," *IEEE Trans. Contr. Syst. Technol.*, vol. 6, no. 1, pp. 111–120, 1998.
[14] T. R. Bewley, "Flow control: new challenges for a new renaissance," *Progress in Aerospace Sciences*, vol. 37, no. 1, pp. 21–58, 2001.
[15] O. M. Aamo and M. Krstić, *Flow Control by Feedback : Stabilization and Mixing*, 1st ed. Great Britain: Springer, 2003.
[16] S. S. Joshi, J. L. Speyer, and J. Kim, "A systems theory approach to the feedback stabilization of infinitesimal and finite-amplitude disturbances in plan poiseuille flow," *J. of Fluid Mechanics*, vol. 332, pp. 157–184, 1997.
[17] ——, "Finite dimensional optimal control of poiseuille flow," *J. Guid. Contr. Dynamics*, vol. 22, no. 2, pp. 340–348, 1999.
[18] L. Cortelezzi, K. Lee, J. Kim, and J. Speyer, "Skin-friction drag reduction via robust-order linear feeback control," *Int. J. Comput. Fluid Dyn.*, vol. 8, no. 1-2, pp. 79–92, 1998.
[19] L. Cortelezzi and J. Speyer, "Robust reduced-order controller of laminar boundary layer transitions," *Physical Review E*, vol. 58, no. 2, pp. 1906–1910, 1998.
[20] A. Emami-Naeini, S. A. McCabe, D. de Roover, J. L. Ebert, and R. L. Kosut, "Active control of flow over a backward-facing step," in *Proc. Conf. Dec. Contr.*, Seville, Spain, 2005, pp. 7366–7371.
[21] P. Christofides and A. Armaou, "Nonlinear control of navier-stokes equations," in *Proc. Amer. Cont. Conf.*, Philadelphia, PA, 1998, pp. 1355–1359.
[22] R. Vazquez and M. Krstic, "A closed-form feedback controller for stabilization of linearized navier-stokes equations: The 2d poisseuille flow," in *Proc. Conf. Dec. Contr.*, Seville, Spain, 2005, pp. 7358–7365.
[23] J. A. Burns and J. Singler, "Feedback control of low dimensional models of transition to turbulence," in *Proc. Conf. Dec. Contr.*, Seville, Spain, 2005, pp. 3140–3145.
[24] T. R. Bewley, P. Moin, and R. Temam, "DNS-based predictive control of turbulence: an optimal benchmark for feedback algorithms," *Journal of Fluid Mechanics*, vol. 447, pp. 179–225, 2001.
[25] K. Butler and B. Farrell, "Three-dimensional optimal perturbations in viscous shear flows," *Physics of Fluids A: Fluid Dynamics*, vol. 4, no. 8, pp. 1637–1650, 1992.

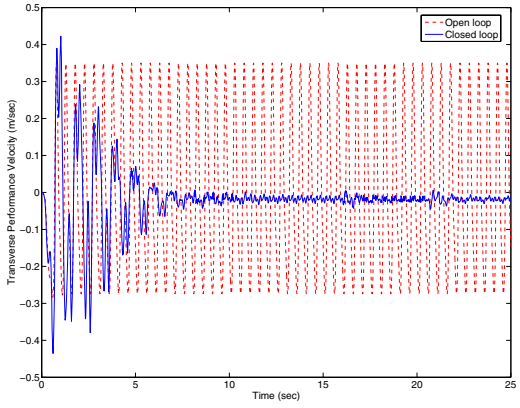

Fig. 7. Open-loop and closed-loop transverse performance velocity response for a dual tone 2 Hz and 6 Hz disturbance rejection with controller order n_c = 12.

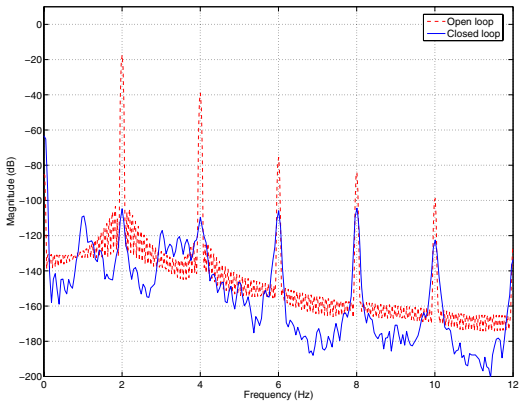

Fig. 8. Open-loop and closed-loop power spectrum for a dual tone 2 Hz and 6 Hz disturbance with controller order n_c = 12. A decrease of more than 80 dB at the disturbance frequency is shown with all other frequency content at least 80 dB below the strongest open loop signal.

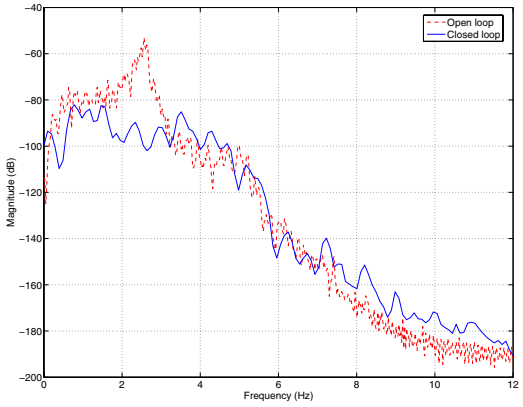

Fig. 9. Power spectrum for band-limited white noise disturbance with controller order n_c = 12. Disturbance rejection of up to 40 dB within the 1.5 Hz to 3 Hz frequency band.

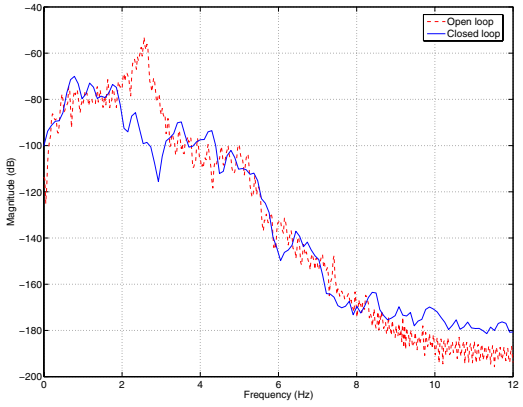

Fig. 10. Power spectrum for band-limited white noise disturbance with controller order n_c = 19. Disturbance rejection of up to 40 dB within the 1.5 Hz to 3 Hz frequency band.